



Cite this: *Green Chem.*, 2023, **25**, 4647


Received 10th March 2023,

Accepted 18th May 2023

DOI: 10.1039/d3gc00820g

rsc.li/greenchem

Evaluation of hybrid amines and alcohol solvent with ion-exchange resin catalysts for energy-efficient CO₂ capture†

Qiang Sun,^a Jia Xiong,^a Hongxia Gao,^{*a} Teerawat Sema,^b Wilfred Olson^a and Zhiwu Liang ^{*a}

The traditional carbon dioxide (CO₂) desorption process in amine-based carbon capture requires high regeneration energy consumption, a factor that has severely limited its application. In this work, cation exchange resin catalysts are tested as a novel approach to accomplish improvement in aqueous monoethanolamine (MEA) regeneration in terms of the CO₂ desorption rate, amount of CO₂ released and relative heat duty. The results indicate that the cation exchange resin Amberlyst-15 significantly increased the amine regeneration rate and improved the amount of CO₂ desorbed by 21%. A possible catalytic mechanism is proposed. In addition, the solvent effects of methanol and ethanol were also explored for low temperature and energy-saving CO₂ desorption technology. In the case of a mixed 12.5 wt% ethanol and 2 wt% Amberlyst-15 catalyst, the system exhibited a reduction of 59% in the energy demand of CO₂ desorption compared with the 5 M MEA baseline. To sum up, this work provides an efficient strategy for MEA regeneration at low temperature, thus reducing the energy consumption for CO₂ capture.

1. Introduction

The continuously rising emission of CO₂ into the atmosphere has resulted in the greenhouse effect, climate changes, and limited the world's ability to accomplish carbon neutrality.^{1,2} CO₂ capture, utilization and storage (CCUS) is regarded as a promising technology to mitigate CO₂ emission and global

warming.^{3–5} Among the post-combustion capture processes, CO₂ capture with amine solvents is currently the best available technology, and has been studied and applied for decades.^{6–8} In a traditional amine solvent CO₂ capture process, the regeneration of the rich-amine solution is carried out above 100 °C.^{9,10} At this temperature, evaporation of water requires the input of a great deal of heat, and thus the energy consumption of the desorption unit contributes more than half of the operation costs.^{11,12} This high energy consumption for amine regeneration and the amine degradation that takes place at high temperature are the main drawbacks which hinder the wide application of amine-based capture technology.^{13,14} Therefore, the development of new CO₂ capture approaches with low energy consumption is necessary.

To reduce the energy consumption of CO₂ capture, various efforts have been developed, such as using new amines^{15,16} and blends of amines,^{17,18} modifying process configurations^{19,20} and using biphasic solvents.^{21,22} Recently, a novel approach for reducing heat duty for MEA regeneration by the application of a solid acid catalyst has been proposed.²³ Previous reports indicated that the addition of a solid acid catalyst could facilitate the rupture of the carbamate C–N bond and accelerate proton transfer, thus decreasing the required regeneration temperature to less than 100 °C.^{24,25} CO₂ desorption at low temperature would eliminate the need for the input of evaporation energy, mitigate amine degradation, and accomplish the utilization of low-temperature waste heat in power plants.^{26,27}

As a result, various solid acid catalysts have been evaluated to promote the CO₂ desorption kinetics at low temperature.²⁸ A brief review of research works for the solvent regeneration process with different catalysts in the rich amine solvent is listed in Table S1.† Zhang *et al.*²⁹ revealed that the molecular sieve catalysts, such as HM, HZ, AO, and Hβ, enhanced the CO₂ desorption rate and decreased the energy consumption required for amine regeneration. Prasongthum *et al.*³⁰ exhibited a superacid catalyst of sulfated metal oxide Ce(SO₄)₂ZrO₂, which had large quantities of Brønsted acid sites and required

^aJoint International Center for CO₂ Capture and Storage (iCCS), Provincial Hunan Key Laboratory for Cost-effective Utilization of Fossil Fuel Aimed at Reducing CO₂ Emissions, College of Chemistry and Chemical Engineering, Hunan University, Changsha, 410082, PR China. E-mail: hxgao@hnu.edu.cn, zwliang@hnu.edu.cn

^bDepartment of Chemical Technology, Faculty of Science, Chulalongkorn University, Bangkok, 10330, Thailand

† Electronic supplementary information (ESI) available: Materials and resin activation; catalyst characterization; details of experimental apparatus and analysis; figures of influence of initial CO₂ loading, influence of catalyst/MEA solvent ratios, influence of methanol concentration, and effects of catalyst and ethanol on CO₂ absorption performance. See DOI: <https://doi.org/10.1039/d3gc00820g>

56% less heat than MEA regeneration. Sahoo *et al.*³¹ investigated an enzyme-coupled matrix of the CA@*fn*-Zn/Fe/MS catalyst, and the addition of this catalyst successfully improved the desorption efficiency by 2.6 times. Bhatti *et al.*³² reported that a series of metal oxides including V₂O₅, MoO₃, WO₃, TiO₂, and Cr₂O₃ could facilitate CO₂ release at a regeneration temperature of 86 °C, and approximately 1.4–2 times greater quantities of CO₂ were released than that in the noncatalytic system. Xing *et al.*¹⁴ synthesized an advanced MOF-derived acid catalyst of SZC@TiO₂ with excellent acidity, which improved the amount of CO₂ released by more than 64.5% and reduced the heat duty for CO₂ desorption.

However, the catalytic regeneration concept is recent and has not been applied in industry, and the variety of catalyst materials still demands to be expanded in this field to identify better catalysts. On the other hand, the existing solid acid catalysts were found to quickly lose their catalytic activity in aqueous systems, and had to be regenerated and activated continuously during circulation.³³ Cation exchange resins are popular heterogeneous catalysts because of their good stability, economy, and ease of recyclability, and have been used in various catalytic reactions, such as esterification, isomerization, alkylation, and acylation.^{34–36} Because cation exchange resins are able to catalyze reactions in the presence of water, and possess acid sites to accelerate proton transfer for carbamate decomposition, they are potential catalysts, and may present excellent catalytic performance and stability in CO₂ desorption processes.

In addition to enhancing CO₂ desorption at low temperature, CO₂ capture capacity is another important factor for low temperature amine regeneration application. As is well known, the introduction of a catalyst can reduce the activation energy and improve the desorption rate while not changing the reaction equilibrium.²⁹ However, at temperatures below 100 °C, the CO₂ loading of the MEA solution after regeneration is still high; thus the cycling capacity is much lower than that in typical industrial application at 0.2–0.25 mol CO₂/mol amine. Various strategies for amine regeneration with large cycling capacity at low temperature have been studied by researchers.^{37–39} Guo *et al.*⁴⁰ investigated the blends of MEA and 2-methoxyethanol (2ME) or 2ethoxyethanol (2EE), which reduced regeneration heat by more than 50%. An aqueous ammonia and organic solvent has been proposed by Novek *et al.*⁴¹ for economically viable carbon capture. Lin *et al.*⁴² reported five absorbents and indicated that low boiling solvent could significantly decrease the energy penalty for regeneration. However, CO₂ desorption with ideal cycling capacity and a fast regeneration rate at low temperature in the MEA system is still a challenge.

In the present work, we combined the advantages of catalytic regeneration and solvent effect to obtain a beneficial method for reducing the regeneration heat. A series of cation exchange resin catalysts were evaluated for their catalytic activity during the CO₂ desorption process. The mixed systems of the catalyst and methanol/ethanol–MEA–water were tested in terms of the desorption rate, cycling capacity, and relative

heat duty in comparison with blank 5 M MEA solution. This result opens up a new avenue for low temperature regeneration with less energy consumption.

2. Experimental

2.1. Materials

The materials used in this work are presented in ESI section 1.†

2.2. Resin activation

The ion exchange resin catalysts were activated by the impregnation method, and the details are listed in ESI section 2.†

2.3. Catalyst characterization

The studied catalysts were characterized by nitrogen physisorption and total acid site analyses. The details of these methods are given in ESI section 3.†

2.4. Experimental apparatus

The experimental apparatus for CO₂ desorption and absorption was used a batch-type setup, and the details of this apparatus are available in ESI section 4 (Fig. S1†).

2.5. Analysis

The evaluation parameters including the CO₂ reaction rate (r , mol (s L)^{−1}), quantity of CO₂ desorbed ($N_{\text{CO}_2, \text{gas}}$, mmol; $N_{\text{CO}_2, \text{liquid}}$, mmol), cycling capacity (mol/mol), heat duty (HD, kJ mol^{−1}) and relative heat duty (RHD, %) were defined, and calculation equations are given in ESI section 5.†

3. Results and discussion

3.1. Structural properties of the catalysts

The catalyst mesoporous surface area, pore volume, pore size and concentration of acid sites are summarized in Table 1. According to Table 1, the mesoporous surface area of the ion exchange resins ranked in the order Amberlyst-15 > Dowex D001 > Amberlyst-35 > Amberlite-732 > Amberlite IR-120, with the surface area of Amberlyst-15 being much larger than those of the other catalysts. As for acid capacity, note that the Amberlyst-15, Amberlite-732, and Amberlyst-35 catalysts displayed similar quantities of acid sites between 3.13 and 3.41 mmol H⁺/g_{cat}, while the Amberlite IR-120 catalyst pos-

Table 1 Textural properties of various catalysts

Catalysts	S_{Meso} (m ² g ^{−1})	V_{pore} (cm ³ g ^{−1})	Pore size (nm)	Acid capacity (mmol H ⁺ /g _{cat})
Amberlyst-15	38.161	0.272	32.98	3.31
Amberlite-732	0.064	0.002	65.47	3.13
Amberlyst-35	2.171	0.012	4.39	3.41
Amberlite IR-120	0.024	0.001	60.19	2.29
Dowex D001	6.608	0.037	1.40	1.93

sessed the lowest acid capacity at 2.29 mmol H⁺/g_{cat}. A previous study reported⁴³ that the mesoporous surface area and acid sites have a positive effect on catalytic performance, because the large surface area enhances the active sites and the acid sites accelerate proton transfer. Therefore, the excellent catalytic performance of Amberlyst-15 can be attributed to the combined effect of the mesoporous surface area and acid capacity.

3.2. Catalytic activity

3.2.1. Influence of catalyst types. The catalytic performance of different resin catalysts for MEA regeneration was evaluated in terms of the CO₂ desorption rate, amount of CO₂ released, and the relative heat duty. CO₂ catalytic performance analysis was conducted by regenerating the CO₂-rich MEA solution with the catalyst at 2 wt%, with the initial CO₂ loading at 0.53 mol CO₂/mol MEA. Fig. 1a displays the CO₂ desorption rate curves with and without the catalyst, and indicates that the reaction kinetics with the four catalysts were all higher than that in the blank run. Among the four catalysts, Amberlyst-15 exhibited the most favorable catalytic activity with the highest desorption rate of 4.192×10^{-4} mol (s L)⁻¹ at 1000 s, which was higher than that observed in the blank run with the highest desorption rate of 3.821×10^{-4} mol (s L)⁻¹ at 1050 s. Thus, it can be concluded that the addition of the catalyst accelerated the desorption rate and shortened the time required to reach the reaction equilibrium, enabling regeneration at a temperature below 100 °C, thereby reducing the evaporation heat required for MEA regeneration.

Fig. 1b indicates the changes in the amount of CO₂ released by the system with the different catalysts and by the noncatalytic system. The quantities of CO₂ released in 1200 s were 110.25, 108.00, 107.50, and 96.00 mmol for Amberlite-732, Amberlyst-35, Amberlite IR-120, and Dowex D001, respectively. The Amberlyst-15 catalyst resulted in the largest amount of CO₂ desorbed at 111.75 mmol in 1200 s, which was 21% higher than that in the blank MEA test. Fig. 1b also exhibits a comparison of the relative heat duty, and it can be seen that the Amberlyst-15 catalyst gave superior performance and the

largest decrease of 17.67% in relative heat duty. In conclusion, the Amberlyst-15 catalyst exhibited the most efficient desorption kinetics and the lowest relative heat duty for CO₂ desorption compared with the other ion exchange resin catalysts, and presents potential for the application of advanced solid acid catalysts in MEA regeneration.

3.2.2. Influence of initial CO₂ loading. It is widely understood that the CO₂ absorbed in MEA solvent is mainly in the forms of HCO₃⁻, CO₃²⁻, and MEACOO⁻. To further investigate the catalytic effect of Amberlyst-15 on CO₂ desorption, the catalytic performance with different initial CO₂ loadings was determined and is shown in Fig. S3a.† Compared with the blank run, the addition of 2 wt% Amberlyst-15 catalyst accelerated the desorption rate under different initial CO₂ loadings.

To investigate the catalytic effect of Amberlyst-15 in the MEA regeneration process, Fig. S4† presents the Raman spectra of the MEA solution, for which the initial CO₂ loading was 0.51 mol CO₂/mol MEA, with and without Amberlyst-15 at various periods. Based on previous reports,⁴⁴ bands located at 1017 cm⁻¹, 1065 cm⁻¹, and 1155 cm⁻¹ were assigned to C–OH stretching (HCO₃⁻), symmetric C–O stretching (CO₃²⁻), and C–N stretching (MEACOO⁻). It was observed that the aforementioned three peak heights decreased more quickly in the presence of the catalyst than in the blank run, which demonstrates that Amberlyst-15 simultaneously promoted the decomposition of carbamate and bicarbonate. This result is in good agreement with the experimental results in section 3.2.4.

3.2.3. Influence of methanol/ethanol concentration. The performance of catalysts in amine regeneration was studied at 90 °C, which is much lower than traditional stripper column temperatures at about 120 °C. As is well known, desorption temperatures below 100 °C would considerably reduce the thermal energy requirement for MEA regeneration, especially sensible heat and evaporation heat. Meanwhile, a low desorption temperature could also reduce the problems caused by high temperature operation, such as amine loss and amine thermal degradation. However, at low temperature, the CO₂ desorption kinetic is slow and the cycling capacity is small, problems that are crucial to solve. The addition of the catalyst

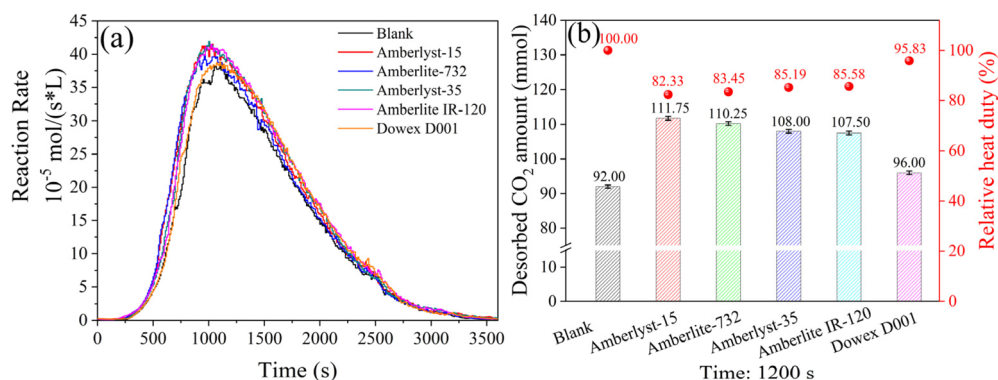


Fig. 1 The CO₂ desorption performance with different catalysts at 90 °C. (a) CO₂ desorption rate curves. (b) Total amount of CO₂ desorbed and relative heat duty at 1200 s.

could significantly optimize the desorption rate to shorten the time taken for reaching reaction equilibrium without changing the thermodynamic equilibrium point of the CO₂ desorption reaction. To further enhance the process, in this section, methanol and ethanol solvents were added into CO₂-rich MEA solution to investigate the solvent effect.

The desorption performance with the variation of methanol concentration from 0 to 20 wt% is given in Fig. S6a–f.† Due to the range limitation of the experimental apparatus, CO₂ desorption experiments were conducted with 300 mL of 5 M CO₂-rich MEA. The heat duty of CO₂ desorption from the blank MEA with and without methanol solvent is presented in Fig. S6f.† It is obvious that the addition of methanol solvent led to significant reduction in energy consumption. The introduction of 20 wt% methanol solvent maximally reduced the heat duty within 1200 s, and reduced the relative heat duty to 43.31% of the blank run. Similar to the regular pattern observed in the desorption rate, the heat duty of CO₂ desorption decreased only slightly with the further addition of methanol to raise the concentration from 15 to 20 wt%. Only considering the cycling capacity, the 20% concentration of the methanol addition presented a superior cycling capacity. However, the more the methanol added, the higher the condensation cost during the absorption and desorption processes. Therefore, based on comprehensive considerations, the optimal MeOH concentration is 15 wt% and thus is used for further studies. Moreover, the addition of 15 wt% methanol decreased the relative heat duty to 45.67%, and is chosen as the optimal concentration for the catalytic performance investigation.

Meanwhile, the CO₂ desorption performance with different mass ratios of ethanol/MEA solvent is displayed in Fig. 2. Fig. 2a indicates the desorption rate curves of five ethanol/MEA solvent ratios, namely 5, 10, 12.5, 15, and 20 wt%, in the MEA regeneration process at 90 °C. It is obvious that the CO₂ desorption rate significantly improved with the addition of ethanol, and that the ethanol solvent facilitated the CO₂ desorbed as compared with the blank run. A linear relationship between the maximum value of the desorption rate and the ethanol/MEA ratio was observed, which indicates that the larger the ethanol/MEA solvent ratio, the faster the desorption rate presented. Among the five different ratios, the 20 wt% ethanol/MEA solvent ratio exhibited the highest maximum value of the desorption rate of 6.253×10^{-4} mol (s L)⁻¹ at 900 s, while the maximum desorption rate value of the MEA blank run is 2.613×10^{-4} mol (s L)⁻¹ at 1120 s. It should be mentioned that the desorption rate was only enhanced slightly when the ethanol/MEA solvent ratio was increased to 12.5 wt%. This indicates that 12.5 wt% is the optimal ratio of ethanol/MEA solvent, because too much ethanol content might aggravate the volatilization of the solvent. Moreover, the addition of the Amberlyst-15 catalyst for the 12.5 wt% EtOH–MEA–water system further increased the maximum desorption rate from 5.685×10^{-4} mol (s L)⁻¹ to 5.757×10^{-4} mol/(s L)⁻¹ compared to the 12.5 wt% EtOH–MEA–water system.

The amount of CO₂ desorbed for MEA solutions with different ethanol/MEA solvent ratios is shown in Fig. 2c and d.

It is notable that the introduction of ethanol increased the quantity of CO₂ released by 60.4% to 208.5% in comparison with the blank run. Thus, the addition of ethanol solvent evidently led to a considerable increase in the amount of CO₂ released, and the amount of CO₂ desorbed increased linearly with an increase in ethanol addition. In this work, the vapor of ethanol and MEA condensed well without obvious loss, but to further decrease the quantity of ethanol lost, a catalyst was introduced to the system to reduce the amount of ethanol addition. As a result, with the addition of 2 wt% Amberlyst-15 catalyst in the optimal ethanol/MEA solvent of 12.5 wt%, the amount of CO₂ desorbed in 1200 s was 118.65 mmol, which is higher than that of the 15 wt% EtOH–MEA–water system. Therefore, the amount of CO₂ desorbed (mmol) in 1200 s was ranked in the order as: blank test (42.45) < 5 wt% EtOH (68.10) < 10 wt% EtOH (93.30) < 12.5 wt% EtOH (110.10) < 15 wt% EtOH (117.30) < 2 wt% Amberlyst-15–12.5 wt% EtOH (118.65) < 20 wt% EtOH (130.95).

The CO₂ loading curves as a function of time and the cycling capacity for different catalyst–EtOH–MEA–water systems are shown in Fig. 2b and e. The cycling capacity of the EtOH–MEA system is 44–256% greater than that of the MEA–water system, which significantly enhances the cycling capacity for CO₂ capture and makes the technology of low-temperature CO₂ desorption possible. It is worth noting that the CO₂ loading of 12.5 wt% EtOH and 2 wt% Amberlyst-15–12.5 wt% EtOH systems tended towards a similar terminal point of about 0.32 mol CO₂/mol MEA. Because the thermodynamic equilibrium mainly depends on the reaction temperature of CO₂ desorption, the introduction of the Amberlyst-15 catalyst can only change the desorption rate rather than the end point of CO₂ loading after MEA regeneration. Meanwhile, in the case of the 2 wt% Amberlyst-15–12.5 wt% EtOH system, the cycling capacity reached 0.194 mol CO₂/mol MEA, which indicated a great improvement of desorption performance for MEA regeneration and about 2.7 times increase compared with the blank run.

Due to the fact that the catalyst–EtOH–MEA–water system desorbed greater amounts of CO₂ during the MEA regeneration process under identical heating conditions, the relative heat duty would decrease accordingly. For a clear comparison, the heat duty of the MEA–water system is taken as a baseline, and the relative heat duty for different ratios of the catalyst–EtOH–MEA–water system are presented in Fig. 2f. The relative heat duty (%) decreased in the sequence: blank test (100) > 5 wt% EtOH (66.23) > 10 wt% EtOH (50.24) > 12.5 wt% EtOH (44.18) > 15 wt% EtOH (42.22) > 2 wt% Amberlyst-15–12.5 wt% EtOH (41.00) > 20 wt% EtOH (39.17), implying that the addition of ethanol solvent reduced the energy consumption by 33.77–60.83%. Moreover, the 2 wt% Amberlyst-15–12.5 wt% EtOH–MEA–water system, which is the optimal system selected, exhibited a reduction of 59.00% in decreasing the energy demand for CO₂ desorption. To sum up, the application of ethanol solvent with the catalyst in the rich-CO₂ MEA regeneration process greatly enhanced the cycling capacity, improved the CO₂ desorption rate and thereby reduced the heat duty requirement.

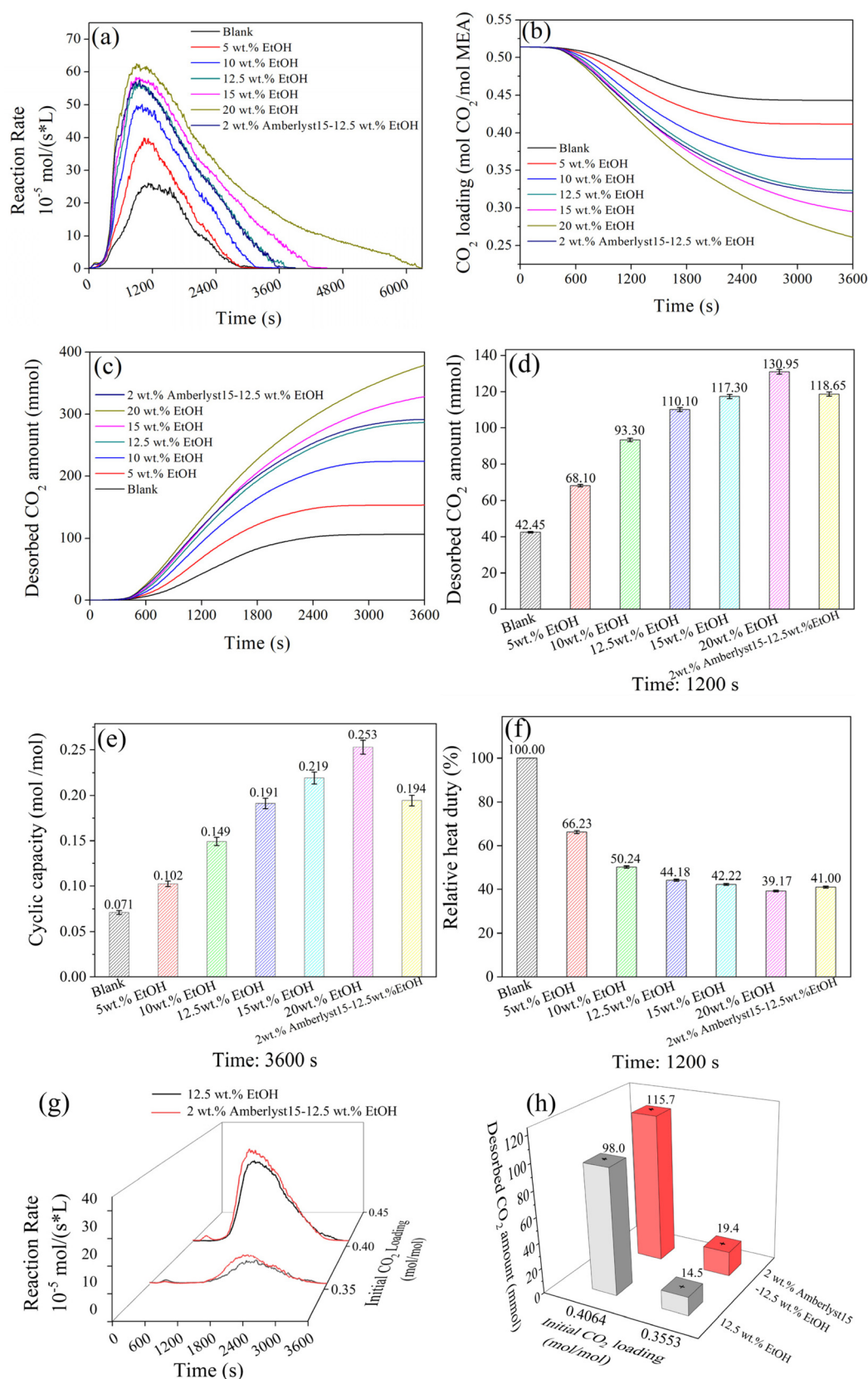


Fig. 2 The CO_2 desorption performance with different ethanol concentrations or initial CO_2 loadings. (a) CO_2 desorption rate curves. (b) CO_2 loading curves. (c) Desorbed CO_2 amount curves. (d) Total amount of CO_2 desorbed at 1200 s. (e) Cyclic capacity. (f) Relative heat duty. (g) CO_2 desorption rate curves. (h) Total amount of CO_2 desorbed at 1200 s.

To further confirm the catalytic performance of Amberlyst-15 in the 2 wt% Amberlyst-15–12.5 wt% EtOH–MEA–water system, the CO₂ desorption performance with different initial CO₂ loadings is displayed in Fig. 2g and h. As can be seen, the Amberlyst-15 catalyst with CO₂ initial loadings of 0.41 and 0.36 mol CO₂/mol MEA increased the quantities of CO₂ released by 18.10% and 33.80%, respectively. Also, it would be valuable work to study the addition of solid catalysts into different packing heights with the blended solvent in the desorber. The catalytic desorption condition with the blended solvent for industrial implementation is in demand for our future work.

3.2.4. Influence of amine types. In order to verify the universality of the benefits of the Amberlyst-15 catalyst in different types of amine desorption processes, the catalyst was introduced into primary, secondary and tertiary amine systems to investigate the catalytic behavior. As listed in Fig. 3, the secondary amines included 2-(methylamino)ethanol (MMEA) and 2-(ethylamino)ethanol (EAE), and the tertiary amines included 2-(diethylamino)ethanol (DEEA), *N,N*-dimethylethanolamine (DMEA) and *N*-methyldiethanolamine (MDEA). The CO₂ desorption capacity of different aqueous amines with and without the Amberlyst-15 catalyst is shown in Fig. 3. It is noteworthy that the Amberlyst-15 catalyst in various amines presented similar catalytic performance, despite the tertiary amine showing a different reaction mechanism, namely the base-catalyzed hydration mechanism compared with the zwitterion mechanism of the primary and secondary amines. It can be seen that the Amberlyst-15 catalyst exhibited no significant catalytic effect in the case of MDEA, which may be due to the too fast MDEA desorption rate, which thereby weakened or overshadowed the catalytic performance. As is well known, tertiary amines only act as the base in a base-catalyzed hydration mechanism, and CO₂ is converted to bicarbonate in the hydrolysis reaction. Thus, in the tertiary amine system, the CO₂ mainly forms HCO₃[−]. On the other hand, in the primary and secondary amines, the main possible forms of CO₂ are MEACOO[−] and HCO₃[−]. Similar catalytic performance results in different amine systems indicated that the Amberlyst-15 cata-

lyst is beneficial for MEACOO[−] and HCO₃[−] breakdown, which is in good agreement with the result of Raman spectra.

3.3. Catalytic mechanism

It is widely accepted that the MEA regeneration process is a zwitterion mechanism proposed by Caplow,⁴⁵ mainly including carbamate breakdown shown in eqn (1) and MEAH⁺ deprotonation shown in eqn (2). Firstly, the carbamate breakdown step is an endothermic reaction that requires large heat inputs, with an activation energy of 15.47 kJ mol^{−1}.⁴⁶ Secondly, the MEAH⁺ deprotonation is also a strongly endothermic reaction with an activation energy of 73.4 kJ mol^{−1}, because water is neutral while the MEA is strongly basic.⁴⁶ Thus, the proton transfer from protonated MEA to water is difficult, and this leads to a barrier of zwitterion formation. Consequently, accelerating the proton transfer in the basic environment is the important key to increase the desorption rate.



In this work, a possible catalytic mechanism with the Amberlyst-15 catalyst is described in Fig. 4. That is, the protons provided by Amberlyst-15 could react with the carbamate and form zwitterions. The unsaturated coordinated ions like SO₄^{2−} on the Amberlyst-15 catalyst attack the nitrogen atom of the carbamate and the delocalized conjugation of the nitrogen atom is converted from sp² to sp³ hybridization. After that, the C–N bond is stretched and weakened, leading to the split of the zwitterion into MEA and CO₂. Moreover, after providing protons the Amberlyst-15 catalyst would act as a basic group and chemisorb with MEAH⁺. Then, the proton transfer from protonated MEA to the deprotonated catalyst and the Amberlyst-15 catalyst is regenerated. As a consequence, the Amberlyst-15 catalyst can enhance the proton transfer in the CO₂ desorption process, thereby decreasing the activation energy for MEA regen-

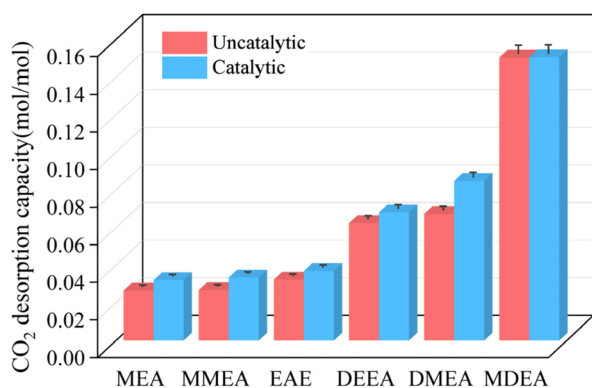


Fig. 3 CO₂ desorption capacity of different amine-based sorbents with and without Amberlyst-15.

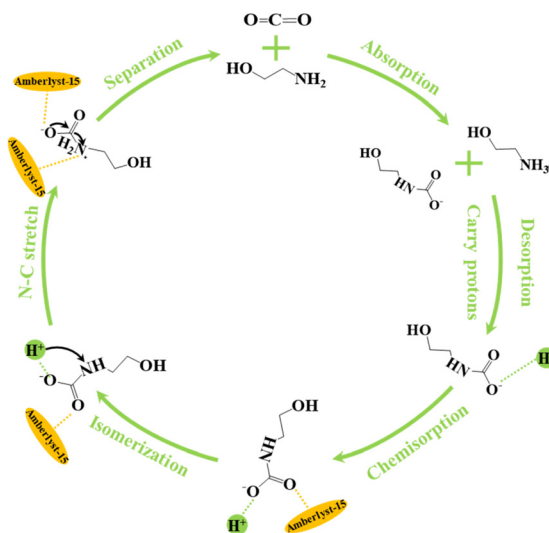


Fig. 4 Possible catalytic mechanism of CO₂ desorption with Amberlyst-15.

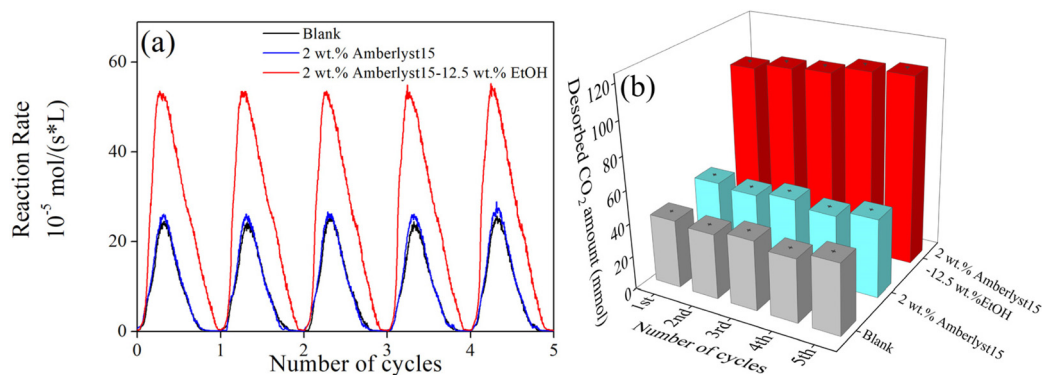


Fig. 5 Stability tests of the 2 wt% Amberlyst-15–MEA–water and 2 wt% Amberlyst-15–12.5 wt% EtOH–MEA–water system. (a) CO_2 desorption rate curves. (b) Total amount of CO_2 desorbed at 1200 s.

eration and improving the desorption rate. These will result in the reduction of time required for the reaction and the decrease of the temperature needed for CO_2 desorption.

3.4. Catalyst reusability

It is well understood that the stability of a catalyst is an important parameter in assessing its overall performance. In this work, five cycles of MEA regeneration were conducted to evaluate the reusability of the Amberlyst-15 catalyst and the ethanol solvent. The cycling test conditions were the same as mentioned earlier. Briefly, 300 mL of CO_2 -rich MEA solution with or without the catalyst and ethanol solvent was regenerated at 90 °C for 3600 s. Then the CO_2 -lean solvent of MEA–water and catalyst–MEA–water systems absorbed CO_2 for 410 s, and the catalyst–EtOH–MEA–water system absorbed CO_2 for 900 s due to the unequal end points of CO_2 loading of the various systems after the CO_2 desorption tests. As a result, the CO_2 loading values of the different systems were all about 0.5 mol CO_2 /mol MEA after each CO_2 absorption step. After that, the CO_2 desorption process was repeated to start the next run. The cycle test results including the desorption rate and CO_2 desorbed amount of catalyst–MEA–water and catalyst–EtOH–MEA–water systems are presented in Fig. 5. As shown in Fig. 5a, there is no obvious change in the CO_2 desorption rate during five cycling experiments, which implies that the Amberlyst-15 catalyst fully retained its catalytic activity and the ethanol solvent was well condensed without apparent loss. Furthermore, it can be seen from Fig. 5b that the desorbed amount of CO_2 over 1200 s for each cycling test did not noticeably decrease, suggesting that both the catalyst–MEA–water system and the catalyst–EtOH–MEA–water system possessed stable cycling capacity. In conclusion, the blended system of catalyst–EtOH–MEA–water exhibited good stability and has the potential for industrial application.

4. Conclusions

The catalytic performance of cation exchange resin in the CO_2 desorption process in terms of the desorption rate,

amount of CO_2 desorbed, and relative heat duty has been investigated at a regeneration temperature of 90 °C. The results indicate that the catalytic performance increased in the order of Amberlite IR-120 < Amberlyst-35 < Amberlite-732 < Amberlyst-15. Moreover, the Amberlyst-15 catalyst has been verified for its universal catalytic activity in different types of amines and is able to catalyze both carbamate and bicarbonate breakdown. Furthermore, it was demonstrated that the solvent effect of ethanol could significantly enhance the cycling capacity to near industrial levels at a low regeneration temperature, which could permit efficient utilization of low-value energy in power plants. It was found that the 2 wt% Amberlyst-15/12.5 wt% EtOH–MEA–water system increased the cycling capacity by about 2.7 times and decreased the relative heat duty by 59%. This study demonstrates that MEA regeneration at low temperature is possible in industrial application.

Conflicts of interest

There are no conflicts to declare.

Acknowledgements

The financial support from the National Key Research & Development Program - Intergovernmental International Science and Technology Innovation Cooperation Project (2021YFE0112800), the National Natural Science Foundation of China (NSFC-No. 22222802, 22138002, 22078083, and 21978075), the Hunan Key R & D Program Project (2020NK2015), the Inner Mongolia Major Science and Technology Major Project (2021ZD0022), the Science and Technology Innovation Program of Hunan Province (2020RC5032), and the China Outstanding Engineer Training Plan for Students of Chemical Engineering & Technology in Hunan University (MOE-No. 2011-40).

References

- 1 Y.-M. Wei, J.-N. Kang, L.-C. Liu, Q. Li, P.-T. Wang, J.-J. Hou, Q.-M. Liang, H. Liao, S.-F. Huang and B. Yu, *Nat. Clim. Change*, 2021, **11**, 112–118.
- 2 J. Rogelj, D. Huppmann, V. Krey, K. Riahi, L. Clarke, M. Gidden, Z. Nicholls and M. Meinshausen, *Nature*, 2019, **573**, 357–363.
- 3 M. Bui, C. S. Adjiman, A. Bardow, E. J. Anthony, A. Boston, S. Brown, P. S. Fennell, S. Fuss, A. Galindo and L. A. Hackett, *Energy Environ. Sci.*, 2018, **11**, 1062–1176.
- 4 B. Verheggen, B. Strengers, J. Cook, R. van Dorland, K. Vringer, J. Peters, H. Visser and L. Meyer, *Environ. Sci. Technol.*, 2014, **48**, 8963–8971.
- 5 L. J. Müller, A. Kätelhön, S. Bringezu, S. McCoy, S. Suh, R. Edwards, V. Sick, S. Kaiser, R. Cuéllar-Franca, A. El Khamlichi, J. H. Lee, N. von der Assen and A. Bardow, *Energy Environ. Sci.*, 2020, **13**, 2979–2992.
- 6 X. Yang, R. J. Rees, W. Conway, G. Puxty, Q. Yang and D. A. Winkler, *Chem. Rev.*, 2017, **117**, 9524–9593.
- 7 N. MacDowell, N. Florin, A. Buchard, J. Hallett, A. Galindo, G. Jackson, C. S. Adjiman, C. K. Williams, N. Shah and P. Fennell, *Energy Environ. Sci.*, 2010, **3**, 1645–1669.
- 8 G. T. Rochelle, *Science*, 2009, **325**, 1652–1654.
- 9 Z. Liang, R. Idem, P. Tontiwachwuthikul, F. Yu, H. Liu and W. Rongwong, *AIChE J.*, 2016, **62**, 753–765.
- 10 X. Zhang, J. Hong, H. Liu, X. Luo, W. Olson, P. Tontiwachwuthikul and Z. Liang, *AIChE J.*, 2018, **64**, 3988–4001.
- 11 X. Zhang, Y. Huang, J. Yang, H. Gao, Y. Huang, X. Luo, Z. Liang and P. Tontiwachwuthikul, *Chem. Eng. J.*, 2020, **383**, 123077.
- 12 H. Gao, Y. Huang, X. Zhang, Z. A. S. Bairq, Y. Huang, P. Tontiwachwuthikul and Z. Liang, *Appl. Energy*, 2020, **259**, 114179.
- 13 Q. Lai, L. Kong, W. Gong, A. G. Russell and M. Fan, *Appl. Energy*, 2019, **254**, 113696.
- 14 L. Xing, K. Wei, Y. Li, Z. Fang, Q. Li, T. Qi, S. An, S. Zhang and L. Wang, *Environ. Sci. Technol.*, 2021, **55**, 11216–11224.
- 15 G. Puxty, R. Rowland, A. Allport, Q. Yang, M. Bown, R. Burns, M. Maeder and M. Attalla, *Environ. Sci. Technol.*, 2009, **43**, 6427–6433.
- 16 Q. Li, H. Gao, S. Liu, J. Lv and Z. Liang, *Chem. Eng. Sci.*, 2020, **218**, 115557.
- 17 H. Liu, X. Zhang, H. Gao, Z. Liang, R. Idem and P. Tontiwachwuthikul, *Ind. Eng. Chem. Res.*, 2017, **56**, 7656–7664.
- 18 H. Shi, L. Zheng, M. Huang, Y. Zuo, S. Kang, Y. Huang, R. Idem and P. Tontiwachwuthikul, *Ind. Eng. Chem. Res.*, 2018, **57**, 11505–11516.
- 19 H. Gao, L. Zhou, Z. Liang, R. O. Idem, K. Fu, T. Sema and P. Tontiwachwuthikul, *Int. J. Greenhouse Gas Control*, 2014, **24**, 87–97.
- 20 Z. Liang, H. Gao, W. Rongwong and Y. Na, *Int. J. Greenhouse Gas Control*, 2015, **34**, 75–84.
- 21 J. Ye, C. Jiang, H. Chen, Y. Shen, S. Zhang, L. Wang and J. Chen, *Environ. Sci. Technol.*, 2019, **53**, 4470–4479.
- 22 X. Zhou, Y. Shen, F. Liu, J. Ye, X. Wang, J. Zhao, S. Zhang, L. Wang, S. Li and J. Chen, *Environ. Sci. Technol.*, 2021, **55**(22), 15313–15322, DOI: [10.1021/acs.est.1c01622](https://doi.org/10.1021/acs.est.1c01622).
- 23 W. Srisang, F. Pouryousefi, P. A. Osei, B. Decardi-Nelson, A. Akachuku, P. Tontiwachwuthikul and R. Idem, *Chem. Eng. Sci.*, 2017, **170**, 48–57.
- 24 D. B. Afari, J. Coker, J. Narku-Tetteh and R. Idem, *Ind. Eng. Chem. Res.*, 2018, **57**, 15824–15839.
- 25 X. Zhang, Z. Zhu, X. Sun, J. Yang, H. Gao, Y. Huang, X. Luo, Z. Liang and P. Tontiwachwuthikul, *Environ. Sci. Technol.*, 2019, **53**, 6094–6102.
- 26 U. H. Bhatti, W. W. Kazmi, H. A. Muhammad, G. H. Min, S. C. Nam and I. H. Baek, *Green Chem.*, 2020, **22**, 6328–6333.
- 27 U. H. Bhatti, H. Sultan, G. H. Min, S. C. Nam and I. H. Baek, *Chem. Eng. J.*, 2020, 127476, DOI: [10.1016/j.cej.2020.127476](https://doi.org/10.1016/j.cej.2020.127476).
- 28 M. S. Alivand, O. Mazaheri, Y. Wu, G. W. Stevens, C. A. Scholes and K. A. Mumford, *ACS Sustainable Chem. Eng.*, 2020, **8**, 18755–18788.
- 29 X. Zhang, Y. Huang, H. Gao, X. Luo, Z. Liang and P. Tontiwachwuthikul, *Appl. Energy*, 2019, **240**, 827–841.
- 30 N. Prasongthum, P. Natewong, P. Reubroycharoen and R. Idem, *Energy Fuels*, 2019, **33**, 1334–1343.
- 31 P. C. Sahoo, M. Kumar, A. Singh, M. P. Singh and S. K. Puri, *Energy Fuels*, 2017, **31**, 11007–11012.
- 32 U. H. Bhatti, A. K. Shah, J. N. Kim, J. K. You, S. H. Choi, D. H. Lim, S. Nam, Y. H. Park and I. H. Baek, *ACS Sustainable Chem. Eng.*, 2017, **5**, 5862–5868.
- 33 X. Zhang, X. Zhang, H. Liu, W. Li, M. Xiao, H. Gao and Z. Liang, *Appl. Energy*, 2017, **202**, 673–684.
- 34 R. Bringué, J. Tejero, M. Iborra, J. F. Izquierdo, C. Fité and F. Cunill, *Chem. Eng. J.*, 2008, **145**, 135–141.
- 35 M. A. Harmer, Q. Sun, A. J. Vega, W. E. Farneth, A. Heidekum and W. F. Hoelderich, *Green Chem.*, 2000, **2**, 7–14.
- 36 A. F. Aguilera, J. Rahkila, J. Hemming, M. Nurmi, G. Torres, T. Razat, P. Tolvanen, K. Eranen, S. Leveneur and T. Salmi, *Ind. Eng. Chem. Res.*, 2020, **59**, 10397–10406.
- 37 F. Barzagli, F. Mani and M. Peruzzini, *Int. J. Greenhouse Gas Control*, 2013, **16**, 217–223.
- 38 C.-H. Yu, T.-W. Wu and C.-S. Tan, *Int. J. Greenhouse Gas Control*, 2013, **19**, 503–509.
- 39 Y. S. Yu, H. F. Lu, T. T. Zhang, Z. X. Zhang, G. X. Wang and V. Rudolph, *Ind. Eng. Chem. Res.*, 2013, **52**, 12622–12634.
- 40 H. Guo, C. Li, X. Shi, H. Li and S. Shen, *Appl. Energy*, 2019, **239**, 725–734.
- 41 E. J. Novek, E. Shaulsky, Z. S. Fishman, L. D. Pfefferle and M. Elimelech, *Environ. Sci. Technol. Lett.*, 2016, **3**, 291–296.

- 42 P.-H. Lin and D. S. H. Wong, *Int. J. Greenhouse Gas Control*, 2014, **26**, 69–75.
- 43 Q. Sun, T. Li, Y. Mao, H. Gao, T. Sema, S. Wang, L. Liu and Z. Liang, *Ind. Eng. Chem. Res.*, 2021, **60**, 18304–18315.
- 44 M. K. Wong, M. A. Bustam and A. M. Shariff, *Int. J. Greenhouse Gas Control*, 2015, **39**, 139–147.
- 45 M. Caplow, *J. Am. Chem. Soc.*, 1968, **90**, 6795–6803.
- 46 H. Shi, A. Naami, R. Idem and P. Tontiwachwuthikul, *Int. J. Greenhouse Gas Control*, 2014, **26**, 39–50.